Biophysical Journal
Article

Biophysical Society

Modeling IP_3-induced Ca^{2+} signaling based on its interspike interval statistics

Victor Nicolai Friedhoff,[1,2] Benjamin Lindner,[3,2] and Martin Falcke[1,2,*]
[1]Max Delbrück Center for Molecular Medicine in the Helmholtz Association, Berlin, Germany; [2]Department of Physics, Humboldt University, Berlin, Germany; and [3]Bernstein Center for Computational Neuroscience Berlin, Berlin, Germany

ABSTRACT Inositol 1,4,5-trisphosphate (IP_3)-induced Ca^{2+} signaling is a second messenger system used by almost all eukaryotic cells. Recent research demonstrated randomness of Ca^{2+} signaling on all structural levels. We compile eight general properties of Ca^{2+} spiking common to all cell types investigated and suggest a theory of Ca^{2+} spiking starting from the random behavior of IP_3 receptor channel clusters mediating the release of Ca^{2+} from the endoplasmic reticulum capturing all general properties and pathway-specific behavior. Spike generation begins after the absolute refractory period of the previous spike. According to its hierarchical spreading from initiating channel openings to cell level, we describe it as a first passage process from none to all clusters open while the cell recovers from the inhibition which terminated the previous spike. Our theory reproduces the exponential stimulation response relation of the average interspike interval T_{av} and its robustness properties, random spike timing with a linear moment relation between T_{av} and the interspike interval SD and its robustness properties, sensitive dependency of T_{av} on diffusion properties, and nonoscillatory local dynamics. We explain large cell variability of T_{av} observed in experiments by variability of channel cluster coupling by Ca^{2+}-induced Ca^{2+} release, the number of clusters, and IP_3 pathway component expression levels. We predict the relation between puff probability and agonist concentration and [IP_3] and agonist concentration. Differences of spike behavior between cell types and stimulating agonists are explained by the different types of negative feedback terminating spikes. In summary, the hierarchical random character of spike generation explains all of the identified general properties.

SIGNIFICANCE Several experimental observations with IP_3-induced Ca^{2+} signaling are not reproduced by current modeling with mean field equations. In general, theories of Physics are highly predictive because they identified the correct mathematical structures to which their subjects correspond, e.g., the mechanics of macroscopic objects to variational principles, the mechanics of microscopic objects to operator theory in Hilbert spaces. The correct identification renders even simple models predictive. We show that perceiving Ca^{2+} signaling as a random walk in the cluster array state space and spike generation as a first passage problem leads to a simple quantitative predictive theory reproducing all general properties of IP_3-induced Ca^{2+} spiking and their robustness properties. This theory might also serve as starting point for derivation of mean field models.

INTRODUCTION

The IP_3-induced Ca^{2+} signaling pathway translates extracellular signals in the form of plasma membrane receptor agonist concentrations into intracellular responses by increasing the cytosolic Ca^{2+} concentration in a stimulus-dependent pattern (1–6). Repetitive sequences of Ca^{2+} spikes are used to regulate many processes in various cell types (1,4,7,8). The concentration increase can be caused either by Ca^{2+} entry from the extracellular medium through plasma membrane channels or by Ca^{2+} release from intracellular storage compartments. In the following, we focus on IP_3-induced Ca^{2+} release from the endoplasmic reticulum (ER), which is the predominant Ca^{2+} release mechanism in many cell types (9). IP_3 sensitizes Ca^{2+} channels (IP_3Rs) on the ER membrane for Ca^{2+} binding, such that Ca^{2+} released from the ER through one channel increases the open probability of neighboring channels (Fig. 1) (10,11). This positive feedback of Ca^{2+} on its own release is called Ca^{2+}-induced Ca^{2+} release (CICR). The released

Submitted March 10, 2023, and accepted for publication June 6, 2023.
*Correspondence: martin.falcke@mdc-berlin.de
Editor: Richard Bertram.
https://doi.org/10.1016/j.bpj.2023.06.004

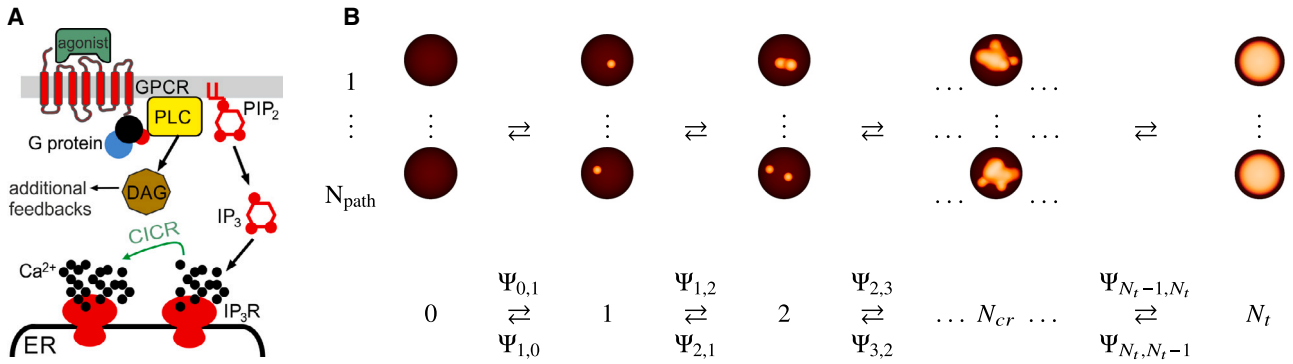

FIGURE 1 (*A*) The inositol 1,4,5-trisphosphate (IP_3) pathway. Binding of agonist to a G-protein-coupled receptor (GPCR) activates phospholipase C (PLC), which produces IP_3 from phosphatidylinositol-4,5-bisphosphate (PIP_2). IP_3 sensitizes IP_3 receptor channels (IP_3Rs) in the membrane of the endoplasmic reticulum (ER) for binding of Ca^{2+}, such that Ca^{2+} released from the ER through one channel increases the open probability of neighboring channels by CICR. Diacylglycerol (DAG) activates in some cell types additional feedbacks to the IP_3R open probability, acting on the timescale of ISI. (*B*) (*Top*) Open clusters are visualized as small filled orange circles. A spike occurs when (almost) all N_t clusters are open. There are N_{path} paths of cluster openings and closing from 0 to N_t open clusters. (*Bottom*) Averaging over all paths leads to a state scheme indexed by the number of open clusters. The transition probabilities $\Psi_{k,k\pm1}$ are explained in the text and Eqs. 3, 4, and 6. To see this figure in color, go online.

Ca^{2+} is removed from the cytosol either by sarco-endoplasmic reticulum Ca^{2+} ATPases into the ER or by plasma membrane Ca^{2+} ATPases into extracellular space.

IP_3Rs are spatially organized into clusters with a variable number of channels from 1 up to about 15. This cluster definition including single channels anticipates that the theory we will formulate is able to account also for channel populations which might not form clusters as suggested by Lock and Parker (12). Clusters are scattered across the ER membrane with reported distances of 1–7 μm (13–17). CICR and Ca^{2+} diffusion couple the state dynamics of the channels. The coupling between channels in a cluster is much stronger than the coupling between adjacent clusters (18).

The structural hierarchy of IP_3R arrangement from the single channel to clusters and cellular cluster arrays is also reflected by the dynamic responses of the intracellular Ca^{2+} concentration as revealed through fluorescence microscopy and simulations (13,19–22). Random openings of single IP_3Rs (blips) may trigger collective openings of IP_3Rs within a cluster (puffs), while Ca^{2+} diffusing from a puff site can then activate neighboring clusters, eventually leading to a global, i.e., cell-wide, Ca^{2+} spike (17,20–23). The timing of blips, puffs, and spikes is random (4,22,24–33). The typical timescale of spiking is the (temporal) average T_{av} of the interspike interval (ISI). Interestingly, that timescale cannot be found in long sequences of puffs from single isolated puff sites (34), i.e., it is an emergent property of the cellular dynamics.

At very strong stimulation, many Ca^{2+} signaling pathways exhibit an increased Ca^{2+} concentration of much longer duration than spikes, which may oscillate (35,36), burst (37,38), or be rather constant (39–41). Typically, the amplitude of these oscillations is smaller than the spike amplitude.

Ca^{2+} exerts also negative feedback on the channel open probability, which acts on a slower timescale than the positive feedback, and has a higher half-maximum value than CICR (13,19,23,34,42–46). This Ca^{2+}-dependent negative feedback helps terminate puffs, and therefore the puff probability immediately after a puff is smaller than the stationary value, but typically not 0 (34). Channel clusters recover within a few seconds to the stationary puff probability in the absence of other negative feedbacks (13,19,23,34,42,43,46–48).

IP_3 is produced by phospholipase C (PLC) upon stimulation of plasma membrane receptors. It sensitizes the IP_3R for Ca^{2+} binding and thus translates the plasma membrane signal into puff probability (11). Ca^{2+}-mobilizing signals are generated by stimuli acting through a large variety of cell-surface receptors, including G-protein and tyrosine kinases-linked receptors (Fig. 1 *A*) (49). Stimulation of these receptors activates other pathways in addition to PLC with plasma membrane receptor-specific feedbacks to IP_3 production and Ca^{2+} release (5,9,49–51,52). They also affect the negative feedback terminating release spikes. Recovery from this negative feedback causes an absolute refractory period T_{min} as part of the ISIs lasting tens of seconds (4,53,54). Hence, the negative feedback that determines the timescale of ISIs is different from the feedback contributing to interpuff interval and requires global (whole-cell) release events.

Earlier stochastic theory of Ca^{2+} signaling focused on certain aspects such as cluster properties and dynamics (47,55–62) or spikes and waves (21,26,63–69) and used simulations and Langevin equations. Recent experimental studies identified general properties of IP_3-induced Ca^{2+} signaling—general in the sense that they apply to all cell types that have been investigated. We list these properties in the next section. Earlier modeling studies did not have this list at their disposal. Most of the general properties are not captured by current theory of IP_3-induced Ca^{2+} signaling. With this study, we would like to advance theory toward capturing these basic properties, and providing

understanding of the stimulation response relation, cell-type-specific behavior, cell variability and at the same time robustness of specific properties. We formulate an approach accounting for this scope and allowing for analytic calculation of moments of the ISI distribution.

Experimental results defining the mathematical theory

Identification of the mathematical structure to which IP_3-induced Ca^{2+} dynamics corresponds requires starting from the basic observations applying to all cells. They are common to all cell types and pathways investigated hitherto. Some of these observations vary quantitatively between individual cells, others do not. We denote by cell variability differences of properties between individual cells of the same type and under the same conditions. We will denote properties that are the same in a quantitative sense for all individual cells of the same type stimulated with the same agonist as cell type and agonist specific. The average interspike interval T^i_{av} and its SD σ^i are calculated as temporal average (temporal SD) over the ISIs of a spike sequence of an individual cell indexed by i. We develop our theory from these experimental observations:

1 Interpuff intervals, puff amplitude, and puff duration are random (34,42,47,70,71).
2 The timescale of Ca^{2+} spiking T_{av} cannot be observed in puff sequences of individual puff sites (34).
3 The sequence of interspike intervals is random (4,24–32,72).
4 The average interspike interval depends sensitively on the strength of spatial coupling by CICR between IP_3R clusters (24,73).
5 The SD σ^i of interspike intervals obeys a linear moment relation to the average ISI T^i_{av}:

$$\sigma^i = \alpha\left(T^i_{av} - T_{min}\right) + \sigma_{min}. \quad (1)$$

The slope α, σ_{min}, and T_{min} are cell type and agonist specific and are not subject to cell variability (4,24–28,73). The slope α is robust against application of a variety of drugs, changing stimulation and buffer addition (4,24,73). σ_{min} is the SD at saturating stimulation.
6 T^i_{av} obeys

$$T^i_{av} = \left(T^i_{ref} - T_{min}\right)e^{-\gamma\Delta[A]^i} + T_{min} \quad (2)$$

with the concentration of extracellular agonist [A], $\Delta[A]^i = [A] - [A]^i_{ref}$, the concentration at the onset of spiking $[A]^i_{ref}$, and the agonist sensitivity γ, which is cell type and agonist specific and is not subject to cell variability (4).
7 Cell variability of the average interspike interval is large. It presents itself as large variability of the average interspike interval at the onset of spiking at low stimulation, and enters the stimulation response relation only via T^i_{ref} (4,24–27,72).
8 Cellular release spikes are terminated by cell-type- and agonist-specific negative feedback. That entails the puff probability immediately after a spike to be smaller than the asymptotic value after recovery from the negative feedback (23,54,74,75).

Puffs and single channel openings (blips) are the noisy microscopic, elemental events, the sum of which constitutes the macroscopic cellular Ca^{2+} transient (observation 1). The amplitude of the noise generated by these elemental events in relation to cellular events is unusually large since each channel opening releases hundreds of Ca^{2+} ions per millisecond. Interpuff intervals are about one-tenth of interspike intervals and local Ca^{2+} concentrations in the vicinity of puffs reach the level of global Ca^{2+} concentrations during a spike. The ratio in size and timescale of macroscopic to microscopic processes for many cellular systems is 10^5 or more, which is sufficient to provide deterministic mean field behavior on cell level, averaging out the microscopic noise. In the case of Ca^{2+} dynamics, that ratio is orders of magnitude smaller and we should not expect noise to average out. Thus, we need a stochastic approach from the start (76).

Puffs and blips are not only the elemental events of Ca^{2+} transients, but also the local dynamics of a reaction-diffusion system. We learn from observation 2 that the local dynamics are nonoscillatory and that IP_3R clusters do not reflect the spiking dynamics, which is an emergent property of the whole cluster array. Observation 3 confirms our expectation that microscopic noise does not average out on cellular level of this reaction-diffusion system. Observation 4 prohibits the formulation of the theory in terms of spatial averages.

We can draw some information on the interspike interval distribution from observation 5. The average T_{av} and SD σ are not independent. This strongly suggests that the process setting T_{av} also sets σ. If we dealt with a noisy deterministic oscillator, some of the parameters setting the noise (σ) would most likely be different from the parameters setting the period, thus preventing a universal relation between average and SD (77,78).

The stimulation response relation is exponential (observation 6). Experiments established the exponential dependency on the agonist concentration not only on the basis of its excellent fits to measured relations but also on the basis of a differential equation $dT_{av}/d[A] = -\gamma\, T_{av}$ derived from stimulation step experiments (4). The experiments also showed that γ does not depend on the agonist concentration [A]. Since this relation is so solidly confirmed, we will use it to parameterize our theory. The agonist sensitivity γ is cell type and agonist specific. Surprisingly, the stimulation response relation (Eq. 2) does not show the canonical behavior close to any bifurcation-generating limit cycles (see Supporting material, section D), indicating that the

onset of spiking does not represent such a bifurcation in mathematical terms.

Cell variability of T_{av} is a basic phenomenon, and is large (observation 7). That poses the question of the meaning of frequency in individual cells. A typical frequency for a given stimulation strength does not exist, but we rather face a distribution of frequencies across individual cells. Surprisingly, cell variability enters the stimulation response relation in a very defined way: as the prefactor of the exponential. Since cell variability is large and a basic observation, modeling needs to account for the distribution of T_{av} from the start and at the same time for the robustness properties of the stimulation response and moment relation.

The negative feedback terminating release spikes mentioned in observation 8 develops once a spike has started, i.e., when the Ca^{2+} concentration is high across the whole cell. It is a global process. It acts on all clusters in the cell simultaneously, and recovery from it also proceeds synchronously for all clusters. Therefore, we can assume spike termination and processes related to this feedback to be much less affected by noise than spike initiation. Hence, it obeys spatially averaged deterministic dynamics.

Defining the theory on the basis of experimental results

We start with formulating a theory for spike generation in a spike sequence. All channels and clusters are closed at the end of a spike (23), because the global negative feedback which terminated the spike has decreased the open probability substantially (observation 8) and started the absolute refractory period. The constant T_{min} in Eqs. 1 and 2 is the sum of spike duration and this absolute refractory period. When T_{min} has passed, channels and clusters start again to open and close sequentially until the next spike terminates. Due to recovery from negative feedback, all cluster opening probabilities increase proportional to $g(1 - I(t))^{n_r}$ from 0 right after T_{min} ($t = 0, I = 1$) to their asymptotic value g ($t = \infty, I = 0$). The inhibitor variable $I(t)$ describes the negative feedback that terminated the previous spike. Its value increases during the spike, and we defined it such that the value is 1 at the time of spike termination. We allow for a dependency of the puff probability on $1 - I(t)$ to n_rth power. If this dependency is cooperative, values of $n_r > 1$ may occur.

The dynamics of the clusters are stochastic (observation 1). Each opening cluster entails a sphere of increased Ca^{2+} concentration around it. We indicate that by the orange spheres in the red round cells in scheme Fig. 1 *B*. The local rise in Ca^{2+} increases the opening probabilities of the open cluster's neighbors due to CICR (observation 4). A spike occurs when (almost) all N_t clusters are open. This state is reached via one of many possible paths of cluster openings from 0 to N_t open clusters. Averaging over all N_{path} paths radically simplifies the system into a state scheme defined by the number of open clusters only (79) (Fig. 1 *B*). The ISI corresponds to the time it takes to get from 0 to N_t open clusters, i.e., it is the first passage time of this random process (78). The first passage time distribution corresponds to the ISI distribution for stationary spike trains.

The transition probabilities from k to $k - 1$ open clusters are determined by the probability that one out of k open clusters closes with rate δ:

$$\Psi_{k,k-1} = k\delta. \tag{3}$$

The probability for the first opening of a cluster is the single-cluster puff probability, $g([IP_3])(1 - I(t))^{n_r}$, times the number of closed clusters (here, simply the total number of clusters, N_t),

$$\Psi_{0,1} = g([IP_3])N_t(1 - I(t))^{n_r} \tag{4}$$

The puff probability is affected by inhibition; it is proportional to the n_rth power of 1-$I(t)$, where the inhibitor variable $I(t)$ decreases from one toward zero after spike termination with the rate λ, i.e.,

$$\frac{dI(t)}{dt} = -\lambda I(t). \tag{5}$$

with the solution $I(t) = e^{-\lambda t}$.

The transition probabilities from k to $k + 1$ open clusters capture the effects of CICR. $[Ca^{2+}]$ increases with the number of open clusters—either in the whole cell or at least in the vicinity of open clusters. We assume this concentration increase to be proportional to the number of open clusters k. Each open cluster increases $[Ca^{2+}]$ by $s_p c_r$ with c_r denoting the resting concentration of $[Ca^{2+}]$. This increase in concentration increases the channel opening rate due to CICR. Thus, CICR increases the transition probabilities from k to $k + 1$ with increasing k. Two factors determine how quickly $\Psi_{k,k+1}$ increases. The first one is the dependency of the channel open probability on $[Ca^{2+}]$. According to a variety of studies, the open probability increases like $[Ca^{2+}]^n = c_r^n(1 + s_p k)^n$ (10,80–84), with reported values for n from 1.0 to 4.0 (1.0 – 2.7 (82), 2.7 (10), 1.6 our fit to data from (83), up to 4.0 (81)). The second factor derives from the picture of spike generation as wave nucleation. The number of closed clusters neighboring the expanding wave increases like the surface of the volume engulfed by the wave, i.e., like $k^{2/3}$. These clusters contribute most to the $[Ca^{2+}]$-mediated increase in open probability. Combining this with the channel open probability dependency on $[Ca^{2+}]$ suggests $n = 1.7 - 4.7$. So, while we are aware that our choice $n = 3$ may not apply to all cell types or situations, we think it covers many situations.

The constant s_p accounts for the strength of spatial coupling and depends on many factors. The level of Ca^{2+} in the ER determines the release current and thus the concentration amplitude of a puff (85). The very geometry of

the cell-wide cluster array sets the distances and thus the $[Ca^{2+}]$ increase due to diffusion. Buffers set the effective diffusion coefficient. This nonexhaustive list illustrates that this CICR-based coupling is a likely candidate for the cause of cell variability. At the same time, the convergence of so many biological parameters on a single parameter of the dynamics is one reason for the robustness and universal properties of Ca^{2+} spiking. Including all factors, we obtain the transition rate from k to $k+1$

$$\Psi_{k,k+1} = g([IP_3])(N_t - k)\left(1 + s_p k\right)^n \left(1 - e^{-\lambda t}\right)^{n_r} \quad (6)$$

comprising the factors (asymptotic single-cluster puff probability g) $\times$ (number of closed clusters $N_t - k$) $\times$ CICR $\times$ (recovery from negative feedback of previous spike). We subsumed the factor c_r^n in g and have chosen $n = 3$ in this study.

The average time for transitions between the states in the linear chain in scheme Fig. 1 is set by the average time of individual cluster interpuff intervals (puff duration) divided by the number of closed (open) clusters. Already the single-cluster puff probability is much higher than the inverse of the average interspike interval and thus $\Psi_{0,1}$ implements observation 2.

The dynamics of the state probabilities is given by the master equation

$$\begin{aligned} \frac{dP_0(t)}{dt} &= \delta P_1(t) - \Psi_{0,1}(t)P_0(t), \\ \frac{dP_k(t)}{dt} &= \Psi_{k-1,k}(t)P_{k-1}(t) + (k+1)\delta P_{k+1}(t) \\ &\quad - (\Psi_{k,k+1}(t) + k\delta)P_k(t), \end{aligned} \quad (7)$$

with $k = 1, \ldots, N_t - 1$. Its Laplace transform defines the difference Eq. S6 for the Laplace transforms of the state probabilities, which we solved analytically by Eq. S7 with $n_r = 1$ (86). Section A in the Supporting material explains how we solved the first passage problem, for which N_t is the absorbing state and $P_{N_t} = 0$ holds. The moments of the ISI distribution are determined by Eqs. S8 and S9. We also simulated trajectories and compare their outcome to the analytical calculations in Fig. S2.

We have introduced our theoretical approach with clusters as stochastic elements. It would have the same structure if we assumed an array of single channels to generate a spike, as the observations by Lock and Parker (12) suggest. The first passage formulation would also apply if we considered very small cells or very fast diffusion, such that the concentration increase caused by open clusters is spatially homogeneous. We could even think of mixed forms, with clusters starting the release and more diffuse single channels joining later, by specifying the $\Psi_{k,k\pm1}$ accordingly.

Summarizing this section, we established the mathematical structure to which we assume IP_3-induced Ca^{2+} spiking corresponds. It is a random walk in the state space of the IP_3R cluster array of a cell with transition rates depending on $[Ca^{2+}]$ and $[IP_3]$. We radically simplified the state space to the number of open clusters.

MATERIALS AND METHODS

Our results are based on analytical calculations using methods derived in Falcke and Friedhoff (86) explained in Supporting material, section A, and stochastic simulations. See Supporting material for more details.

RESULTS

From puffs to spikes

Puffs and blips are the elemental release events, and they are only observed at low stimulation (13,19,20) or at very weak spatial coupling (87–89). The transition from this regime to spiking happens when stimulation increases the puff probability. Fig. 2 illustrates the transition from puffs to spikes. It shows the average first passage time from all clusters closed at the end of the absolute refractory period T_{min} to N open clusters ($N \leq N_t$) and relates it to the single-cluster puff probability g. Considering events of a given amplitude, i.e., a given N, all of them become more frequent with increasing puff probability.

Single-cluster openings occur after about 10 s at very low values of g (with the parameter values in Fig. 2), but it takes a hundred or more seconds until two clusters are open at the same time and even longer for three open clusters or a spike. In the time sequence of events, we would see many puffs

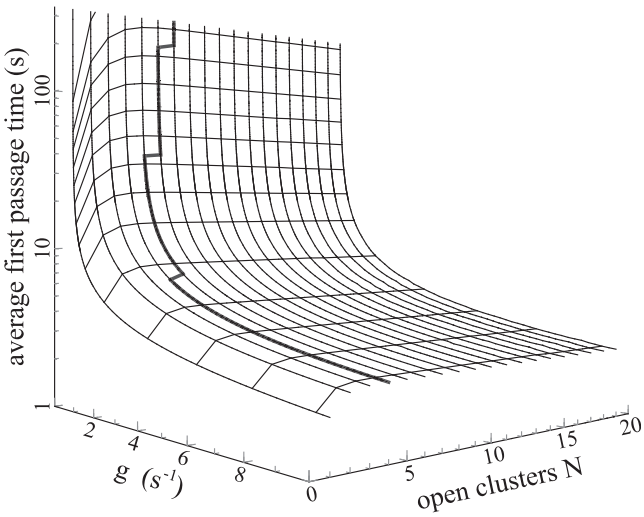

FIGURE 2 Dependence of the average first passage time from 0 to N open clusters on the single-cluster puff probability g. The value of g is the puff probability after complete recovery from the previous spike. The parameters used are $\lambda = 0.001443\ s^{-1}$, $s_p = 1.7$, and $N_t = 30$. Saturation of the average first passage time in dependence on N starts at $N = N_{cr}(g)$, which is marked by the thick line. The state N_{cr} is defined as the lowest state N for which $\langle FPT(N+1)\rangle / \langle FPT(N)\rangle - 1 < 0.02$ holds, i.e., the first state N for which the average first passage time does not increase by more than 2% w.r.t. to reaching the next highest state.

before a larger event happens. At large values of g, puffs are still a few times more frequent than events involving more clusters. But the time until large N values are reached is short and spikes happen soon after the absolute refractory period.

The process of spike generation becomes more tangible by following the average first passage time with increasing N at a given large puff probability in Fig. 2. The first passage time essentially saturates at a certain number of open clusters N_{cr}. Once this value N_{cr} is reached by the random cluster opening, almost all clusters open in next to no time due to the strong positive feedback of CICR to the cluster opening rate. The existence of $N_{cr} \leq N_t$ corresponds to the experimental observation that opening of a few clusters starts a global spike with almost certainty (21,70,90,91) (see also here: https://parkerlab.bio.uci.edu/images_movies_presentations/calcium.htm).

The dependency of T_{av} on cluster-cluster coupling and cluster number

We explained above that the many factors setting the strength of spatial coupling between IP_3R clusters converge on the parameter s_p. Fig. 3 illustrates the relation between T_{av} and s_p. We see that T_{av} depends on the strength of spatial coupling (observation 4) described by the parameter s_p.

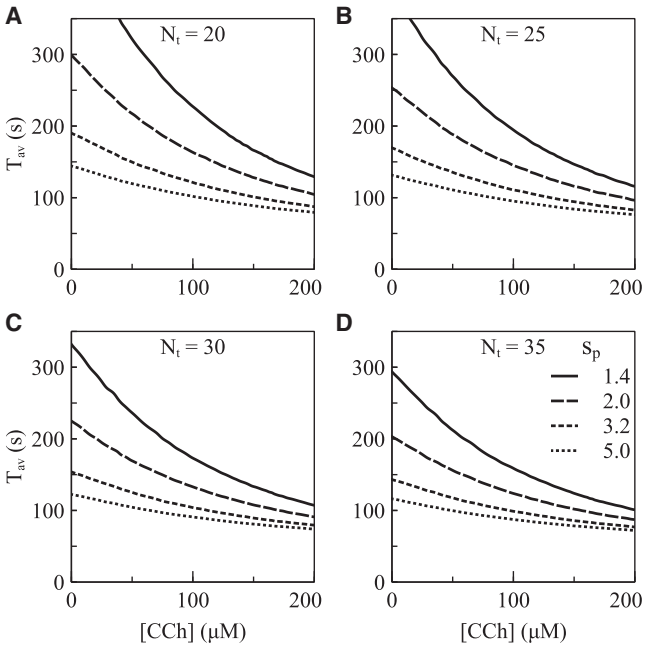

FIGURE 3 The average interspike interval is affected by the strength of spatial coupling s_p and the number of clusters in the cell N_t. The four panels show T_{av}([CCh]) for HEK cell parameters for four N_t values and four s_p values. The smaller the value of s_p—and therefore the weaker the spatial coupling—the larger is T_{av}. Note that T_{av} responds more sensitively to a change of s_p from 2.0 to 1.4 than from 5.0 to 3.2. T_{av} decreases with increasing N_t as a comparison across panels for equal s_p values shows. The legend in (*D*) applies to all panels. CCh, carbachol.

The dependency of T_{av} on Ca^{2+} diffusion properties has been investigated by Skupin et al. (24) by measuring T_{av} before and after addition of the Ca^{2+} buffers BAPTA or EGTA to spiking cells. They substantially reduce the concentration of free Ca^{2+} in the vicinity of open channels, corresponding to a decrease of s_p (18). Only a part of cells resumed spiking after buffer addition, and mostly those with small T_{av} before buffer was added. T_{av} of those continuing to spike increased by a factor of 1.7 on average. The examples in Fig. 3 cover this range of T_{av} change. T_{av} is most sensitive to s_p changes in the range of small s_p values. Cells in that range most likely correspond to the fraction of cells in the experiments which did not resume spiking after buffer addition.

The total cluster number in the cell N_t is the other geometrical parameter affecting T_{av}. T_{av} decreases with increasing cluster number N_t (Fig. 3). With a dependency of rates on numbers, increasing the cell size, while keeping the IP_3R concentration constant decreases T_{av} (see (21,22) for simulations). That is one of the fundamental differences to models based on mean field dynamics exhibiting a dependency of rates on concentrations.

The slope of the moment relation

The moment relation Eq. 1 has been confirmed for all cell types and pathways investigated so far. Its linearity is an important constraint on mathematical models. The value of the slope α is determined by the timescale of recovery from the negative feedback terminating release spikes (79). In combination with its robustness properties mentioned above, meaning independence from many other parameters, it contains valuable information on the pathways coactivated with PLC by cell stimulation (see Fig. 1).

We identify α with the coefficient of variation (CV) of the underlying stochastic process, given by $CV = \alpha = (\sigma^i - \sigma_{min})/(T^i_{av} - T_{min})$. The range of possible values for α is therefore between 0 for a deterministic spiking process and 1 for a homogeneous Poisson process. The experimentally determined value of HEK cells for a variety of CCh (carbachol) concentrations and coapplication of other drugs varied in a rather small range between 0.20 and 0.28 (4). We consider α as robust and not being subject to cell variability on that basis. Consequently, the main determinant of the value of α can only be other parameters not being subject to cell variability. Indeed, the rate of recovery from negative feedback λ and the exponent n_r, which are not subject to cell variability, turned out to be the main determinants (79).

We used α and the range of observed T_{av} values as fit criteria to determine the value of λ applying to the different cell types and agonists (Table 1). All experimental data could be fit with $n_r = 1$. The moment relations resulting from these fits are shown in Fig. 4. Note, the slower the recovery from negative feedback (the smaller λ), the smaller

TABLE 1 Parameter values varying between pathways and cell types, resulting from fits to measured values of α, T_{av} ranges and T_{av} ([A])

Pathway	λ (s^{-1})	Θ (s)	T_{min} (s)
HEK cells, CCh	1.443×10^{-3}	3.68	57
Hepatocytes, Pe	1.154×10^{-2}	1.39	61
Hepatocytes, Vp	6.0×10^{-4}	6.91	44
Salivary gland, 5-HT	1.154×10^{-3}	3.83	16
Astrocytes, spont.	4.0×10^{-1}		54

Agonists are carbachol (CCh), phenylephrine (Pe), vasopressin (Vp), and serotonin (5-HT). Astrocytes spiked spontaneously. Parameter Θ is the contribution of the stochastic process to T_{min} (Eq. S13). Parameter values identical for all cell types are: $\delta = 6.93\ s^{-1}$ (71, 92), $n = 3$ (Eq. 6) (10, 80–84), $[IP_3]_0 = 0.01$ ms UV flash, $k_p = 0.016\ ms^{-1}$ (Eq. 8) (71), $g_0 = 5.0\ s^{-1}$ (Eq. 8) (34), $n_r = 1$ (Eqs. 4 and 6). Parameters describing cell variability are $s_p = 1.0 - 5.0$ and $N_t = 15 - 45$ (Eq. 6). Their value ranges have been chosen to match observed T_{av} ranges. We consider g_0 as cell type and agonist specific (see text). However, since we do not have measured values for the Pe, Vp, and 5-HT pathways, we fixed g_0 to a value agreeing with HEK data (34) and allowing to describe the observations in all four pathways. The same applies to $[IP_3]_0$.

the value of α (86). The α values for astrocytes, HEK cells, and hepatocytes stimulated with Pe or Vp could all be fit with the exponent $n_r = 1.0$ in the recovery factor (Table 1).

The value of α is surprisingly robust. Addition of buffer, coapplication of drugs with stimulation, which changed IP_3 production, IP_3 sensitivity of the IP_3R or ER Ca^{2+} uptake, and varying stimulation all changed T_{av}, but not α (4,24,73). Modeling the robustness of α requires first to remind us of likely properties of cell variability. We discussed before that all the factors setting the strength of spatial coupling s_p and the number of clusters N_t are likely candidates for causing cell variability. Expression levels of the components of the IP_3 pathway like the plasma membrane receptor or PLC most likely also vary between individual cells causing cell variability in agonist sensitivity and the relation between puff probability and agonist concentration $g([A])$. Indeed, it is a common observation that individual cells start to spike at different stimulation strength. That means in terms of the model that the value of $[A]^i_{ref}$ in Eq. 2 varies between cells (as index i indicates), which is analogous to a variation of T^i_{ref}.

Fig. 4, *E–G*, shows the moment relation with HEK cell parameters for ranges of parameter values describing cell variability. N_t, s_p and $[A]^i_{ref}$ have been varied to obtain cell variability. In addition, we vary the ranges from which we sample s_p and [CCh]. Fig. 4 *H* shows the value of α for the range of [CCh] used in experiments. The value of α stays always well within the measured range. These results demonstrate that our theory reproduces the robustness properties of α.

The relation between puff probability and agonist concentration and the exponential stimulation response relation

We quantify the relation of the puff probability to the agonist concentration by matching the measured stimulation response relation $T_{av}([A])$ (Eq. 2) with the analytically calculated relation $T_{av}(g)$ (see Fig. 2; Eqs. S9 and S12–S15): $T_{av}(g) = T_{av}([A])$ relating g to [A] via the T_{av} values. Solving that equation for g provides the dependency of the puff probability g on agonist concentration [A], $g([A])$. The $g([A])$ obtained with the measured stimulation response relations $T_{av}([A])$ from (4) are shown in Fig. 5, *A–D*. They have been determined with typical values of s_p and N_t for each cell type. We call them for later use reference relations.

As expected, g increases with stimulation in all cases. We determine $g([A])$ for the agonist concentration range covered by the measured stimulation response relations. If these relations do not saturate within the range of measured agonist concentrations, neither does $g([A])$. That applies to HEK cells, salivary gland cells, and hepatocytes stimulated with Vp in Fig. 5. Stimulating hepatocytes with increasing concentration of Pe leads to saturation of T_{av} at T_{min} at a few μM. These cells still spike at 50 μM, and the corresponding relation $g([Pe])$ saturates and has a sigmoidal shape.

We use $g([A])$ to learn more about the stimulation response relation, now. The population average of the experimentally measured stimulation response relation can be fit by a single exponential (4) (see Eq. 2). That strongly suggests that this relation for all individual cells obeys essentially the same exponential function, which is not affected by cell variability (4). Cell variability enters only by the prefactor of the exponential $T^i_{ref} - T_{min}$. The surprising aspects of this observation are that, given all the obvious cell variability among the pathway components, the exponential relation is not violated, all cells have the same value of γ and that cell variability enters so well-defined via the prefactor only.

There is no indication or a priori reason to assume that the parameters causing cell variability are correlated in a way guaranteeing the exponential relation and the value of γ, such as that cells with small N_t have a very sensitive IP_3 pathway to compensate for the small cluster number. Rather, the ability to fit the concentration response relations for a range of the parameter values describing cell variability with the same relation $g([A])$ and by varying the prefactor $T^i_{ref} - T_{min}$ of the exponential only is compatible with our ideas on cell variability. We use the reference relation $g([A])$ determined above to verify this ability of our theory.

We show stimulation response relations for four different pathways calculated from the stochastic process (see Eq. S16) in Fig. 6. The full line in each panel corresponds to the measured relation in Thurley et al. (4). It is exactly reproduced by definition of the reference $g([A])$. Other line styles show stimulation response relations with other values of cell variability parameters than the reference relation. The exponential relation with the measured agonist sensitivity γ is a very good approximation for the stimulation response relations of cells with different values of s_p and N_t than the reference relation in all four cases in Fig. 6.

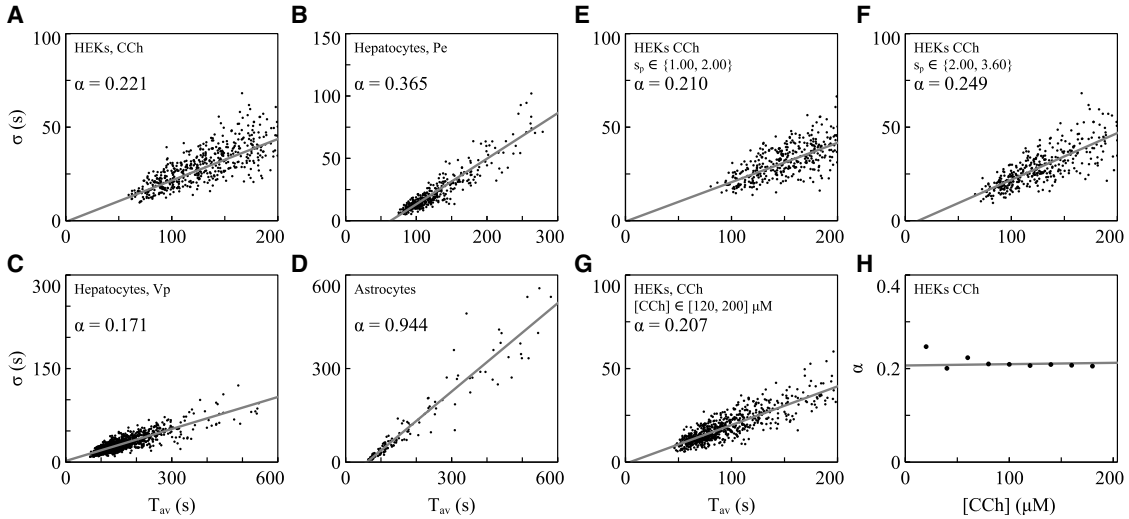

FIGURE 4 Moment relation Eq. 1 between the average ISI T_{av} and the ISI SD σ for four pathways. Parameter values are listed in Table 1. (*A*) HEK cells stimulated with [CCh] ∈ [20, 100] μM. The measured range of α is 0.20–0.28 (4). (*B*) Hepatocytes stimulated with Pe. The measured value of α is 0.37 (4). (*C*) Hepatocytes stimulated with Vp. The measured value of α is 0.17 (4). (*D*) Spontaneously spiking astrocytes. The measured range of α is 0.94 − 1.01 (73). Analogous to the analysis of experimental data in (4,73), averages over 12 consecutive ISIs sampled from simulations were used for each data point. Data points differ in N_t and s_p. (*E* and *F*) σ-T_{av} plot for the HEK cells, α has been determined with different s_p values while all N_t are included and [CCh] as in (*A*). α varies slightly but stays in the experimentally measured range, showing that it is a robust property of the system w.r.t. to a change of factors affecting s_p. (*G*) σ-T_{av} plot for HEK cells with the same parameters as in (*A*) apart from the stimulation range which is now [CCh] ∈ [120, 200] μM. (*H*) α changes only slightly with agonist concentration and stays within the measured range. Data points for a given [CCh] value were determined with σ and T_{av} values averaged over a stimulation range [CCh] ± 20%. Fig. S4 shows α for different ISI sample sizes.

Variability in $[A]^i_{ref}$ does not cause deviations from the exponential dependency. It is analogous to variability in T^i_{ref} due to the properties of the exponential function in agreement with the experimental results. Hence, our theory is able to explain the robustness properties of the stimulation response relation observed by Thurley et al. (4) without assuming compensating correlations between the parameters of cell variability.

While the exponential dependency on agonist in $T_{av}([A])$ was an input to our theory, the robustness properties of $T_{av}([A])$ were not. Therefore, we consider the finding that they are met by our theory as a confirmation of our choices.

The relation between [IP_3] and agonist concentration

Binding of agonist to a G-protein-coupled receptor (GPCR) activates PLC, which produces IP_3 diffusing to the IP_3R and sensitizing the receptor for binding of activating Ca^{2+} (Fig. 1 *A*). Knowledge about the concentration of the intracellular messenger IP_3 was not required for the results presented so far, since we know the stimulation response relation of T_{av}. Indeed, we need additional experimental information to be able to make statements on [IP_3]. According to our approach starting from puff probability, we invoke the relation between [IP_3] and puff probability measured by Dickinson et al. (71). The expression

$$g([IP_3]) = g_0\left(1 - e^{-k_p\left([IP_3]+[IP_3]_0\right)}\right) \tag{8}$$

is a very good fit to the data in Dickinson et al. (71). It is set up to [IP_3] in units of UV flash duration used in experiments uncaging caged IP_3. Dickinson et al. measured in SH-SY5Y cells with a maximum puff probability g_0 of about 1 s^{-1}. The measurements by Thurley et al. suggest it to be up to five times larger in HEK293 cells (34). Hence, we expect the maximum puff probability g_0 to be specific to the agonist and cell type.

We can now determine the relation between [IP_3] and agonist concentration, [IP_3]([A]), by inverting Eq. 8 to provide [IP_3](g) and using g([A]) for [IP_3]([A]) = [IP_3](g([A])) (Fig. 7). This is an effective description of the behavior of the GPCR and PLC controlling IP_3 production. The same remarks as for g([A]) with regard to the agonist concentration range and saturation behavior apply to [IP_3]([A]). We see sigmoidal behavior for [IP_3]([Pe]) (Fig. 7 *B*). This saturating type of relation is typical for the response of signaling pathways. The other three pathways do not saturate within the agonist concentration range available for the fit. However, their shape is compatible with sigmoidal functions saturating at larger concentrations, maybe beyond the spiking in the overstimulation regime. We used g([A]) to derive [IP_3]([A]). That guarantees consistency with the relation between puff probability g and T_{av} as well as the stimulation response relation Eq. 2. The red line in Fig. 6 *E* shows this consistency for the reference case.

We expect cell variability also in the expression level of the components of the pathway leading to IP_3 production like, e.g., the GPCR, G protein, and PLC (see Fig. 1 *A*).

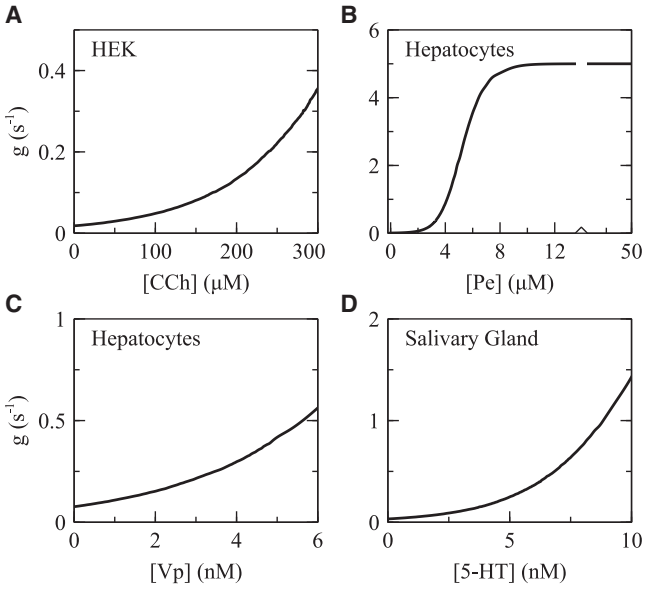

FIGURE 5 (*A–D*) Single-cluster puff probability g versus agonist concentration for four pathways. The stimulation response relation Eq. 2 saturates for hepatocytes stimulated with Pe, and so does $g([\mathrm{Pe}])$. The stimulation response relation does not saturate with the other three pathways, and therefore $g([\mathrm{A}])$ does not saturate within the spiking regime either.

However, in contrast to the moment relation and the stimulation response relation, we do not have experimental data verifying this assumption or quantifying the robustness properties. Therefore, we are limited to theoretical considerations. We expect the stimulation response relation to exhibit robustness with regard to changes of some properties of the IP_3 pathway, but also to reflect the cell type and agonist specificity of γ, i.e., some properties of the IP_3 pathway will affect γ.

The expression level of IP_3 pathway components fixes the saturation value $[IP_3]_{max}$ of $[IP_3]([A])$ (see Fig. 7 *B*). Fig. 6 *E* shows $T_{av}(g([IP_3]([A])))$ with doubled $[IP_3]_{max}$. It can be fit very well with the same exponential as the reference case. Changing the saturation value from 70 to 200% of its reference value affects mainly the prefactor and the agonist sensitivity γ by $\pm 10\%$ only (Figs. S5 and S6). Hence, the expression level of the pathway components affects the stimulation response relation in good agreement with its robustness properties in a large range of $[IP_3]_{max}$. Interestingly, $T_{av}(g([IP_3]([A])))$ was more robust against an increase of $[IP_3]_{max}$ than a decrease. We investigated whether values of the parameters determining $[IP_3]([A])$ exist, providing more robustness against decreasing $[IP_3]_{max}$. Fig. S5 shows that this clearly is the case. Increasing either k_p or g_0 extends the robust range toward small $[IP_3]_{max}$. However, a definite statement on the robustness properties requires more experimental research to position measured $[IP_3]([A])$ in parameter space.

The sensitivity of the pathway is determined by molecular properties such as the specific type of GPCR, tyrosine kinase, and PLC involved (11), which are not subject to cell variability. The sensitivity of $[IP_3]([A])$ should therefore affect elements of our theory with the same robustness properties. That is what we observe when we double the sensitivity of $[IP_3]([A])$ by use of $[IP_3](2[A])$. Thus doubles the agonist sensitivity of the stimulation response relation γ according to our expectations (Fig. 6 *E*).

Mathematically, $g([IP_3]([A]))$ transforms $T_{av}(g)$ into the stimulation response relation. Since $g([IP_3])$ (Eq. 8) and the stimulation response relation (Eq. 2) are fixed by experimental results, the outcome of the stochastic process of spike generation $T_{av}(g)$ (Fig. 2) shapes $[IP_3]([A])$. The result that $[IP_3]([A])$ has a sigmoidal shape as we expect for a signaling pathway and is compatible with the robustness properties of the stimulation response relation are confirmations for the assumption that spike generation is a first passage process.

DISCUSSION

Our theory describes the complete pathway from the agonist concentration to the Ca^{2+} spiking characteristics. Stimulation with agonist produces $[IP_3]$ according to the relations shown in Fig. 7. That entails a puff probability $g([IP_3]([A]))$ according to Eq. 8. The value of the puff probability finally entails an average interspike interval according to the relation $T_{av}(g([IP_3]([A])), s_p^i, N_t^i, [A]_{ref}^i)$ calculated from the stochastic process of spike generation with examples shown in Fig. 2. The parameters s_p^i, N_t^i, and $[A]_{ref}^i$ account for cell variability and specify individual cells. The complete pathway model is in agreement with all the eight general observations listed above and additionally with Eq. 8.

Cell variability of T_{av} is large. At the same time, it is an important source of information on the relations defining IP_3-induced Ca^{2+} spiking quantitatively and their robustness properties. We established the moment relation and stimulation response relation by exploiting the cell variability found in experiments (4,24). In this study, we used the robustness properties revealed by the features not being subject to cell variability as crucial information for verifying and parameterizing our theory. Cellular parameters with given robustness properties can only be related to parameters with equal or even more general robustness. This is a criterion for defining parameter relations. We confirmed it for the agonist sensitivity γ by showing that it does not depend on the cell variability parameters. We exploited it by fixing the recovery rate λ with the slope α of the moment relation.

Cell-type- and agonist-specific properties enter the theory by three experimentally determined parameter values. The moment relation provides the slope α corresponding to the CV of the stochastic part of the interspike interval $T_{av} - T_{min}$. Since α depends on the recovery rate λ and is independent of many other parameters due to its

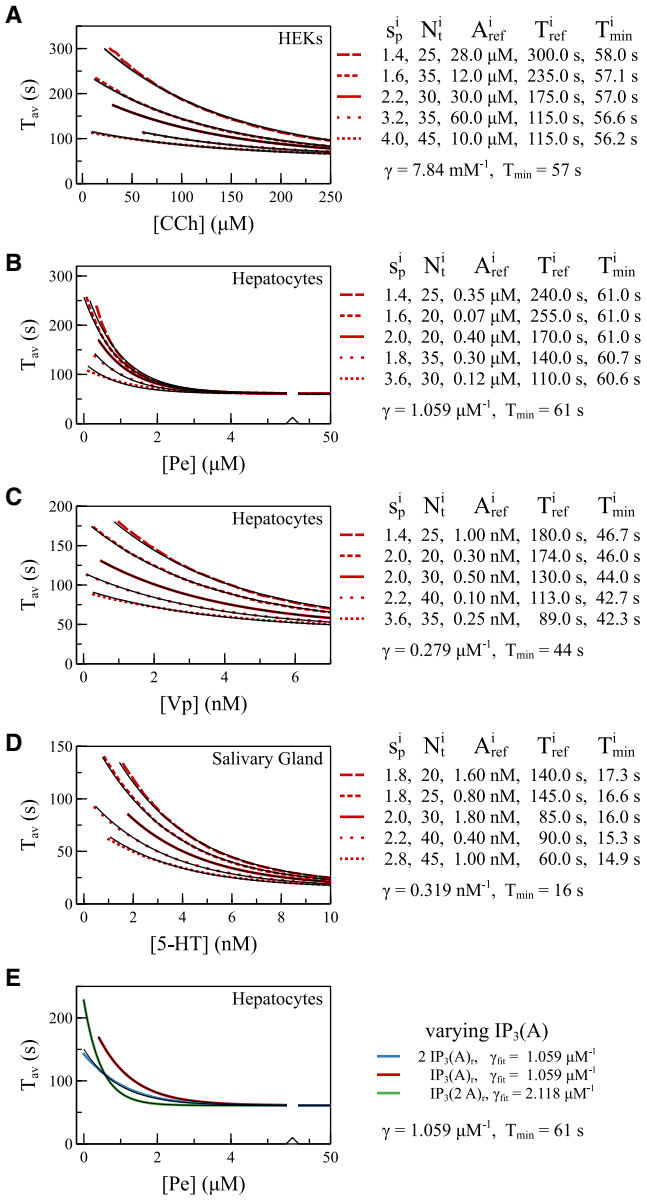

FIGURE 6 (*A–D*) $T_{av}([A])$ for different pathways and different combinations of N_t and s_p are shown. Red lines are fits to exponential functions as Eq. 2 in observation 6. Black lines are calculated from the stochastic process of spike generation and the reference relation $g([A])$ as $T_{av}(g([A]), s_p^i, N_t^i)$, i.e., we first calculate g from [A] (Fig. 5, *A–D*) and then $T_{av}(g, s_p^i, N_t^i)$ (Fig. 2). The data shown by solid lines use the reference values for s_p and N_t. They fit the experimental data from (4) perfectly by definition. All other lines use different values of s_p and N_t but the same reference $g([A])$. Fits are exponential functions from Eq. 2 in observation 6 using the pathway specific value for γ for all lines, and T_{ref}^i and T_{min}^i as fit parameters. Hence, the curves differ in T_{ref} and by small amounts in T_{min}^i. Since the variability of T_{min}^i is much smaller than the values of T_{min}^i, we consider T_{min} as not being subject to cell variability. The quality of the fits illustrates that the stimulation response relations of a given pathway for different cell variability parameter values can be very well approximated by the same exponential and T_{min} values. That reproduces the robustness properties of the measured stimulation response relations. (*E*) We show $T_{av}(g([IP_3]([A])), s_p, N_t)$ by black lines, i.e., we first calculate $[IP_3]$ from [A], then g from $[IP_3]$ (Eq. 8), and then $T_{av}(g)$. In addition, we show the effect of a twofold expression level of the IP_3 pathway by $T_{av}(g(2[IP_3]([A])), s_p, N_t)$, and $T_{av}(g([IP_3](2[A])), s_p, N_t)$ for doubled sensitivity. All calculations use the reference values for s_p and N_t. Colored lines show exponential fits. Doubling the sensitivity of $[IP_3]([A])$ doubles the value of γ.

robustness properties, we use the value of α to determine λ. The stimulation response relation contributes the value of the agonist sensitivity γ and the absolute refractory period T_{min}. They determine the relation between single-cluster puff probability and agonist concentration $g([A])$, and affect via Eq. 8 also $[IP_3]([A])$.

We have chosen the parameters s_p, N_t, and $[A]_{ref}$ (or T_{ref} instead of $[A]_{ref}$) to describe cell variability. The choice of s_p and N_t is obvious from the vast experimental literature showing puff sites in individual cells. The value ranges have been chosen to match the observed T_{av} ranges. The common experience that individual cells start spiking at individual agonist concentrations is picked up by cell-specific $[A]_{ref}$.

Our theory comprises additional parameters which we kept constant in this study: n, n_r, δ, k_p, $[IP_3]_0$, g_0 (see Table 1). We kept the cluster closing rate δ constant across all cell types and pathways, since recent studies showed that all IP_3R isoforms produce similar puffs (93,94). n, δ, and k_p are fixed by experimental results (see Table 1).

The parameter Θ describes the contribution of the stochastic process to T_{min}. It is related to g_0 and therefore a prediction following from the choice for g_0. If g_0 is very large, the first passage time is very small at saturating stimulation and the stochastic process contributes little to T_{min}. An experimental value of g_0 is known for HEK cells (Table 1) but not for hepatocytes and salivary gland cells. Hence, only the Θ value for HEK cells follows from measured values.

IP_3-induced Ca^{2+} spiking generates spikes in a hierarchical process and exhibits randomness on all structural levels. Our theory starts from these observations. Spiking in general obeys the linear moment relation (Eq. 1) and the exponential stimulation response relation (Eq. 2), IP_3-induced puffs obey Eq. 8, and so does our theory including the corresponding robustness characteristics. These relations are mechanistically unrelated observations without theory. Calculating $T_{av}(g)$ from the stochastic first passage process was sufficient to provide a quantitative picture connecting all three relations and predicting the relation between puff probability g and stimulation [A], $g([A])$, and $[IP_3]$ and stimulation $[IP_3]([A])$.

Comparing modeling concepts

Early modeling concepts of intracellular Ca^{2+} signaling pioneered mathematical modeling in cellular physiology (80,84,95–97). They derived mean field differential equations directly from the master equation of channel state dynamics and the concentration dynamics of the cytosol and ER. These approaches average master equations on (sub)

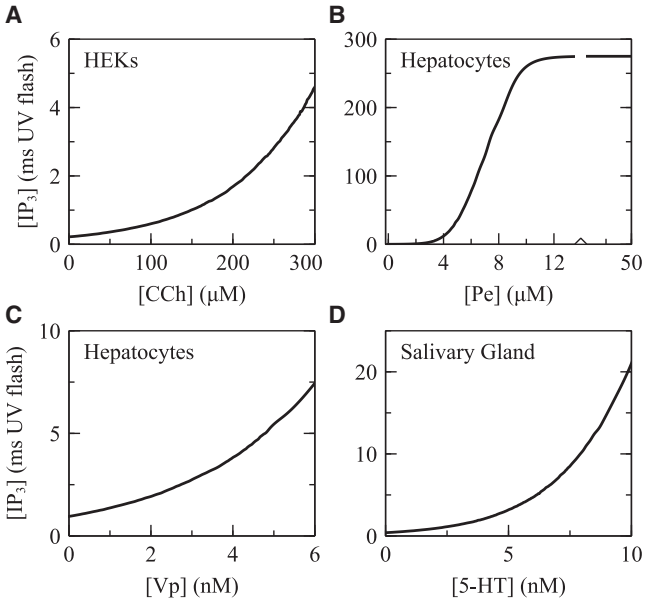

FIGURE 7 (*A–D*) The dependency of $[IP_3]$ on agonist concentration [A], $[IP_3]([A])$, for four different pathways obtained by inverting Eq. 8 and using the reference puff probability agonist relations $g([A])$ from Fig. 5.

cellular level. This study suggests a theoretical concept not requiring the deterministic limit. So, are there actually differences in the predictions of early mean field theory to our approach, with conceptual distinctions causing them? We would like to discuss a few examples for differences here. They illustrate which approximations we accept, when we use the mean field limit of stochastic models.

Input and output of theories

Mean field theories typically fit mean field models to population averages and provide trajectories and bifurcation schemes as output. They relate specific parameter values to specific behavioral characteristics. Our approach uses ranges or distributions of parameter values capturing cell variability as input and uses specific parameters for cell-type- and agonist-specific properties only. It provides distributions of behavioral characteristics, which are generated by noise and cell variability, as output.

The origin of timescales

The representation of the ISI timescale in deterministic models requires necessarily a process realizing that timescale (84,98,99). Slow recovery from negative feedback is one example of such a process. However, spontaneous spiking behavior of astrocytes illustrates that the ISI timescale may arise in stochastic models without a corresponding process. As we know from the measured value of the slope of the moment relation α close to 1 (Fig. 4 *D*), the timescale of recovery from negative feedback in astrocytes is much shorter than the average interspike interval (Fig. 4 *D*; Table 1), and the cell reaches a stationary state soon after a spike. Noise generates the next spike out of this stationary state. If the spike generation probability is small, it takes long before the next spike happens. This long timescale arises from the small value of the spike generation probability. It does not arise from a *slow process* on the cell level. When we derive mean field equations for such a system, they do not exhibit spiking and the noise generated timescale is lost. Fitting time constants of putative slow processes to T_{av} leads to erroneous conclusions on mechanisms in these cases. Mean field approaches are not able to capture slow timescales in the generation of individual spikes arising from small probabilities.

The relation of rates and timescales to system parameters and variables

Cases such as the astrocytes are identified by $\alpha \approx 1$. The case $\alpha < 1$ means spikes occur during the recovery from negative feedback. Since noise strongly affects the spike initiation during the transient, the ISI timescale is not proportional to λ^{-1} but depends, e.g., for the asymptotically symmetric random walk on λ like $\lambda^{-\nu}$ with ν varying from 1/2 to close to 1 when N_t changes from 1 to large values (86). This dependency on the cell variability parameter N_t indicates a potential cell variability of the dependency of the ISI timescale on the relaxation rate.

Rates in mean field equations are proportional to (products of) concentrations according to the law of mass action. Eqs. 3, 4, 5, and 6 and Figs. 3 and 6 show that rates of stochastic processes are proportional to numbers. Thus, mean field approaches predict spike frequencies to be independent of cell size, stochastic approaches can easily explain a dependency on cell size. Mean field equations predict the onset of spiking as bifurcations generating limit cycles (52,99–101), which entail canonical behavior of the period of spiking close to onset (see Supporting material, section D). The stimulation response relation does not correspond to any of these canonical relations. The strength of spatial coupling drops out of mean field equations spatially averaging on cell level. However, we see again from Eqs. 3, 4, 5, and 6, Figs. 3 and 6, and the experimental results in Skupin et al. (24) that strength of spatial coupling affects timescales sensitively. While we could imagine mean field approaches taking spatial coupling strength by some effective approximations into account, stochastic approaches have the advantage of working with clusters as discrete entities and thus can naturally accommodate for coupling strength parameters.

CONCLUSION

Our concept as basis for a comprehensive theory

Our concept not only explains the basic observations, but also defines how to include more detail. The fact that we needed to vary only λ and T_{min} to capture the ISI statistics of four different pathways illustrates the potential for detail

that can be included. For example, more detail on $[IP_3]([A])$ could be included by varying k_p, $[IP_3]_0$, g_0, and n_r. Cell variability in expression levels of pathway components determining $[IP_3]([A])$ appears likely to us. Addressing it in the model would require some experimental data to which we could fit the model parameters. Alternative descriptions of CICR and cluster structure can be included by the choice of the CICR factor in Eq. 6 and its dependency on the number of open clusters or channels.

We focused here on puff properties and interspike intervals, since they are sufficient to present the essence of our theory, and the general observations 1–8 refer to them. The transition rates Eqs. 3 and 6 and the master Eq. 7 define a random walk in the state space of the cellular cluster array, which is the mathematical structure of IP_3-induced Ca^{2+} signaling. They also define the starting point for a more comprehensive theory. The analytical solution Eqs. S6–S8 is not limited to the first passage problem for which we used it. Refining $I(t)$ dynamics (replacing the simple linear dynamics Eq. 5 we have chosen here) would be the means to include more detailed characteristics of recovery from negative feedback after spike termination and to describe complex signal patterns like bursting (102–104). Including processes during the spike in simulations of the model to address spike shape and bursting is straightforward. Accepting the approximations discussed above, we can also derive mean field models from Eq. 7. Hence, we think our approach is able to accommodate the full complexity of Ca^{2+} signals and a variety of modeling concepts (84, 105).

SUPPORTING MATERIAL

Supporting material can be found online at https://doi.org/10.1016/j.bpj.2023.06.004.

AUTHOR CONTRIBUTIONS

M.F. designed the research. V.N.F. carried out all computations and simulations, and wrote data evaluation tools. M.F. and B.L. supervised the research. V.N.F., M.F., and B.L. wrote the article.

ACKNOWLEDGMENTS

V.N.F. has been supported by DFG grant Fa350/13-1 (to M.F.). B.L. acknowledges support by DFG grant LI 1046/4-1. We thank the reviewers for a very constructive review process.

DECLARATION OF INTERESTS

The authors declare no competing interests.

REFERENCES

1. Berridge, M. J., M. D. Bootman, and P. Lipp. 1998. Calcium - a life and death signal. *Nature.* 395:645–648.
2. Taylor, C. W. 1995. Why do hormones stimulate Ca^{2+} mobilization. *Biochem. Soc. Trans.* 23:637–642.
3. Thul, R., T. C. Bellamy, …, S. Coombes. 2009. Calcium oscillations. *In* Cellular Oscillatory Mechanisms. 641 of *Advances In Experimental Medicine And Biology, volume*. M. Maroto and N. A. M. Monk, eds Springer New York, pp. 1–27.
4. Thurley, K., S. C. Tovey, …, M. Falcke. 2014. Reliable encoding of stimulus intensities within random sequences of intracellular Ca^{2+} spikes. *Sci. Signal.* 7:ra59.
5. Dupont, G., L. Combettes, …, J. W. Putney. 2011. Calcium oscillations. *Cold Spring Harbor Perspect. Biol.* 3, a004226.
6. Schipke, C. G., A. Heidemann, …, H. Kettenmann. 2008. Temperature and nitric oxide control spontaneous calcium transients in astrocytes. *Cell Calcium.* 43:285–295.
7. Schulman, H., P. I. Hanson, and T. Meyer. 1992. Decoding calcium signals by multifunctional CaM kinase. *Cell Calcium.* 13:401–411.
8. Li, W., J. Llopis, …, R. Y. Tsien. 1998. Cell-permeant caged $InsP_3$ ester shows that Ca^{2+} spike frequency can optimize gene expression. *Nature.* 392:936–941.
9. Taylor, C. W., and P. Thorn. 2001. Calcium signalling: IP_3 rises again and again. *Curr. Biol.* 11:R352–R355.
10. Bezprozvanny, I., J. Watras, and B. E. Ehrlich. 1991. Bell-shaped calcium-response curves of Ins(1,4,5)P - and calcium-gated channels from endoplasmatic reticulum of cerebellum. *Nature.* 351:751–754.
11. Berridge, M. J. 1993. Inositol trisphosphate and Calcium signalling. *Nature.* 361:315–325.
12. Lock, J. T., and I. Parker. 2020. IP_3 mediated global Ca^{2+} signals arise through two temporally and spatially distinct modes of Ca^{2+} release. *Elife.* 9, e55008.
13. Bootman, M., E. Niggli, …, P. Lipp. 1997. Imaging the hierarchical Ca^{2+} signalling in HeLa cells. *J. Physiol. (London).* 499:307–314.
14. Smith, I. F., S. M. Wiltgen, and I. Parker. 2009. Localization of puff sites adjacent to the plasma membrane: functional and spatial characterization of Ca^{2+} signaling in SH-SY5Y cells utilizing membrane-permeant caged IP_3. *Cell Calcium.* 45:65–76.
15. Taufiq-Ur-Rahman, A. Skupin, …, C. W. Taylor. 2009. Clustering of $InsP_3$ receptors by $InsP_3$ retunes their regulation by $InsP_3$ and Ca^{2+}. *Nature.* 458:655–659.
16. Suhara, W., M. Kobayashi, …, K. Mikoshiba. 2006. Visualization of inositol 1,4,5-trisphosphate receptor by atomic force microscopy. *Neurosci. Lett.* 391:102–107.
17. Keebler, M. V., and C. W. Taylor. 2017. Endogenous signalling pathways and caged IP_3 evoke Ca^{2+} puffs at the same abundant immobile intracellular sites. *J. Cell Sci.* 130:3728–3739.
18. Thul, R., and M. Falcke. 2004. Release currents of IP_3 receptor channel clusters and concentration profiles. *Biophys. J.* 86:2660–2673.
19. Yao, Y., J. Choi, and I. Parker. 1995. Quantal puffs of intracellular Ca^{2+} evoked by inositol trisphosphate in Xenopus oocytes. *J. Physiol.* 482:533–553.
20. Marchant, J., N. Callamaras, and I. Parker. 1999. Initiation of IP_3 -mediated Ca^{2+} waves in Xenopus oocytes. *EMBO J.* 18:5285–5299.
21. Falcke, M. 2003. On the role of stochastic channel behavior in intracellular Ca^{2+} dynamics. *Biophys. J.* 84:42–56.
22. Skupin, A., H. Kettenmann, and M. Falcke. 2010. Calcium signals driven by single channel noise. *PLoS Comput. Biol.* 6, e1000870.
23. Marchant, J. S., and I. Parker. 2001. Role of elementary Ca^{2+} puffs in generating repetitive Ca^{2+} oscillations. *EMBO J.* 20:65–76.
24. Skupin, A., H. Kettenmann, …, M. Falcke. 2008. How does intracellular Ca^{2+} oscillate: by chance or by the clock? *Biophys. J.* 94:2404–2411.
25. Perc, M., A. K. Green, …, M. Marhl. 2008. Establishing the stochastic nature of intracellular calcium oscillations from experimental data. *Biophys. Chem.* 132:33–38.

26. Dupont, G., A. Abou-Lovergne, and L. Combettes. 2008. Stochastic aspects of oscillatory Ca^{2+} dynamics in hepatocytes. *Biophys. J.* 95:2193–2202.

27. Dragoni, S., U. Laforenza, …, F. Moccia. 2011. Vascular endothelial growth factor stimulates endothelial colony forming cells proliferation and tubulogenesis by inducing oscillations in intracellular Ca^{2+} concentration. *Stem Cell.* 29:1898–1907.

28. Cao, P., X. Tan, …, J. Sneyd. 2014. A deterministic model predicts the properties of stochastic calcium oscillations in airway smooth muscle cells. *PLoS Comput. Biol.* 10, e1003783.

29. Croft, W., K. Reusch, …, T. C. Bellamy. 2016. Probabilistic encoding of stimulus strength in astrocyte global calcium signals. *Glia.* 64:537–552.

30. Tilūnaitė, A., W. Croft, …, R. Thul. 2017. A Bayesian approach to modelling heterogeneous calcium responses in cell populations. *PLoS Comput. Biol.* 13:1–25.

31. Powell, J., M. Falcke, …, R. Thul. 2020. A statistical view on calcium oscillations. *Adv. Exp. Med. Biol.* 1131:799–826.

32. Oprea, L., N. Desjardins, …, A. Khadra. 2022. Characterizing spontaneous Ca2+ local transients in OPCs using computational modeling. *Biophys. J.* 121:4419–4432.

33. Jung, P., D. Swaminathan, and A. Ullah. 2010. Calcium spikes: chance or necessity? *Chem. Phys.* 375:625–629 (in honor of Peter Hänggi).

34. Thurley, K., I. F. Smith, …, M. Falcke. 2011. Timescales of IP_3 -evoked Ca^{2+} spikes emerge from Ca^{2+} puffs only at the cellular level. *Biophys. J.* 101:2638–2644.

35. Berridge, M. J. 1990. Calcium oscillations. *J. Biol. Chem.* 265:9583–9586.

36. Nash, M. S., K. W. Young, …, S. R. Nahorski. 2001. Receptor-specific messenger oscillations. *Nature.* 413:381–382.

37. Green, A. K., P. H. Cobbold, and C. J. Dixon. 1994. Elevated intracellular cyclic AMP exerts different modulatory effects on cytosolic free Ca^{2+} oscillations in single rat hepatocytes. *Biochem. J.* 302:949–955.

38. Green, A. K., C. J. Dixon, …, M. J. Fisher. 1993. Adenine dinucleotide-mediated cytosolic free Ca^{2+} oscillations in single hepatocytes. *FEBS.* 322:197–200.

39. Nash, M. S., M. J. Schell, …, R. A. J. Challiss. 2002. Determinants of metabotropic glutamate receptor-5-mediated Ca^{2+} and inositol 1,4,5-trisphosphate oscillation frequency. *J. Biol. Chem.* 277:35947–35960.

40. Bootman, M. D., C. W. Taylor, and M. J. Berridge. 1992. The thiol reagent, thimerosal, evokes Ca^{2+} spikes in HeLa cells by sensitizing the inositol 1,4,5-trisphosphate receptor. *J. Biol. Chem.* 267:25113–25119.

41. Jouaville, L. S., F. Ichas, …, J. D. Lechleiter. 1995. Synchronisation of calcium waves of mitochondrial substrates in Xenopus laevis oocytes. *Nature.* 377:438–441.

42. Parker, I., J. Choi, and Y. Yao. 1996. Elementary events of $InsP_3$ -induced Ca^{2+} liberation in Xenopus oocytes: hot spots, puffs and blips. *Cell Calcium.* 20:105–121.

43. Higgins, E. R., H. Schmidle, and M. Falcke. 2009. Waiting time distributions for clusters of IP3 receptors. *J. Theor. Biol.* 259:338–349.

44. Gin, E., M. Falcke, …, J. Sneyd. 2009. A kinetic model of the inositol trisphosphate receptor based on single-channel data. *Biophys. J.* 96:4053–4062.

45. Wagner, L. E., II, and D. I. Yule. 2012. Differential regulation of the InsP3 receptor type-1 and -2 single channel properties by InsP3, Ca^{2+} and ATP. *J. Physiol. (London).* 590:3245–3259.

46. Mak, D.-O. D., J. E. Pearson, …, J. K. Foskett. 2007. Rapid ligand-regulated gating kinetics of single inositol 1,4,5-trisphosphate receptor Ca^{2+} release channels. *EMBO Rep.* 8:1044–1051.

47. Fraiman, D., B. Pando, …, S. P. Dawson. 2006. Analysis of puff dynamics in oocytes: interdependence of puff amplitude and interpuff interval. *Biophys. J.* 90:3897–3907.

48. Wang, X., Y. Hao, …, G. D. Smith. 2015. Ca_{2+} -activation kinetics modulate successive puff/spark amplitude, duration and inter-event-interval correlations in a Langevin model of stochastic Ca^{2+} release. *Eye Sci.* 264:101–107.

49. Berridge, M. J., P. Lipp, and M. D. Bootman. 2000. The versatility and universality of calcium signalling. *Nat. Rev. Mol. Cell Biol.* 1:11–21.

50. Bird, G. S., M. F. Rossier, …, J. W. Putney, Jr. 1993. Sinusoidal oscillations in intracellular calcium due to negative feedback by protein kinase C. *J. Biol. Chem.* 268:8425–8428.

51. Bartlett, P. J., W. Metzger, …, A. P. Thomas. 2015. Differential regulation of multiple steps in inositol 1,4,5-trisphosphate signaling by protein kinase C shapes hormone-stimulated Ca^{2+} oscillations. *J. Biol. Chem.* 290:18519–18533.

52. Politi, A., L. D. Gaspers, …, T. Höfer. 2006. Models of IP_3 and Ca^{2+} oscillations: frequency encoding and identification of underlying feedbacks. *Biophys. J.* 90:3120–3133.

53. Woods, N. M., K. S. Cuthbertson, and P. H. Cobbold. 1986. Repetitive transient rises in cytoplasmic free calcium in hormone-stimulated hepatocytes. *Nature.* 319:600–602.

54. Rooney, T. A., E. J. Sass, and A. P. Thomas. 1989. Characterization of cytosolic calcium oscillations induced by phenylephrine and vasopressin in single fura-2-loaded hepatocytes. *J. Biol. Chem.* 264:17131–17141.

55. Shuai, J. W., and P. Jung. 2002. Stochastic properties of Ca^{2+} release of inositol 1,4,5-trisphosphate receptor clusters. *Biophys. J.* 83:87–97.

56. Shuai, J. W., and P. Jung. 2003. Optimal ion channel clustering for intracellular calcium signaling. *Proc.Nat.Acad.Sci.USA.* 100:506–510.

57. Shuai, J., J. E. Pearson, …, I. Parker. 2007. A kinetic model of single and clustered IP_3 receptors in the absence of Ca^{2+} feedback. *Biophys. J.* 93:1151–1162.

58. Nguyen, V., R. Mathias, and G. D. Smith. 2005. A stochastic automata network descriptor for Markov chain models of instantaneously-coupled intracellular Ca^{2+} channels. *Bull. Math. Biol.* 67:393–432.

59. Thul, R., and M. Falcke. 2006. Frequency of elemental events of intracellular Ca^{2+} dynamics. *Phys. Rev. E.* 73, 061923.

60. Cao, P., G. Donovan, …, J. Sneyd. 2013. A stochastic model of calcium puffs based on single-channel data. *Biophys. J.* 105:1133–1142.

61. Cao, P., M. Falcke, and J. Sneyd. 2017. Mapping interpuff interval distribution to the properties of inositol trisphosphate receptors. *Biophys. J.* 112:2138–2146.

62. Rüdiger, S., P. Jung, and J.-W. Shuai. 2012. Termination of Ca^{2+} release for clustered IP_3 R channels. *PLoS Comput. Biol.* 8, e1002485.

63. Keizer, J., and G. D. Smith. 1998. Spark-to-wave transition: saltatory transmission of calcium waves in cardiac myocytes. *Biophys. Chem.* 72:87–100.

64. Dawson, S. P., J. Keizer, and J. E. Pearson. 1999. Fire-diffuse-fire model of dynamics of intracellular calcium waves. *Proc.Nat.Acad.Sci.USA.* 96:6060–6063.

65. Keizer, J., G. D. Smith, …, J. E. Pearson. 1998. Saltatory propagation of Ca^{2+} waves by Ca^{2+} sparks. *Biophys. J.* 75:595–600.

66. Bär, M., M. Falcke, …, L. S. Tsimring. 2000. Discrete stochastic modeling of calcium channel dynamics. *Phys. Rev. Lett.* 84:5664–5667.

67. Wang, K., W.-J. Rappel, and H. Levine. 2004. Cooperativity can reduce stochasticity in intracellular Ca^{2+} dynamics. *Phys. Biol.* 1:27–34.

68. Lopez, L., E. Piegari, …, S. Ponce Dawson. 2012. Intracellular calcium signals display an avalanche-like behavior over multiple length-scales. *Front. Physiol.* 3:350.

69. Ramlow, L., M. Falcke, and B. Lindner. 2023. An integrate-and-fire approach to Ca^{2+} signaling. Part I: Renewal model. *Biophys. J.* 122:713–736, in press.

70. Bootman, M. D., M. J. Berridge, and P. Lipp. 1997. Cooking with calcium: the Recipes for composing global signals from elementary events. *Cell.* 91:367–373.

71. Dickinson, G. D., D. Swaminathan, and I. Parker. 2012. The probability of triggering calcium puffs is linearly related to the number of inositol trisphosphate receptors in a cluster. *Biophys. J.* 102:1826–1836.

72. Sauer, H., C. Hofmann, …, J. Hescheler. 1998. Spontaneous calcium oscillations in embryonic stem cell-derived primitive endodermal cells. *Exp. Cell Res.* 238:13–22.

73. Skupin, A., and M. Falcke. 2007. Statistical properties and information content of calcium oscillations. *Genome Inform.* 18:44–53.

74. Cobbold, P. H., A. Sanchez-Bueno, and C. J. Dixon. 1991. The hepatocyte calcium oscillator. *Cell Calcium.* 12:87–95.

75. Sneyd, J., K. Tsaneva-Atanasova, …, D. I. Yule. 2006. A method for determining the dependence of calcium oscillations on inositol trisphosphate oscillations. *Proc. Nat. Acad. Sci. USA.* 103:1675–1680.

76. Friedhoff, V. N., L. Ramlow, …, M. Falcke. 2021. Models of stochastic Ca^{2+} spiking. *Eur. Phys. J. Spec. Top.* 230:2911–2928.

77. Skupin, A., and M. Falcke. 2009. From puffs to global Ca^{2+} signals: how molecular properties shape global signals. *Chaos.* 19, 037111.

78. van Kampen, N. 2001. Stochastic Processes in Physics and Chemistry. North-Holland, Amsterdam.

79. Thurley, K., and M. Falcke. 2011. Derivation of Ca^{2+} signals from puff properties reveals that pathway function is robust against cell variability but sensitive for control. *Proc Nat Acad Sci USA.* 108:427–432.

80. De Young, G. W., and J. Keizer. 1992. A single-pool inositol 1,4,5-trisphosphate-receptor-based model for agonist-stimulated oscillations in Ca_{2+} concentration. *Proc.Natl.Acad.Sci USA.* 89:9895–9899.

81. Marchant, J. S., and C. W. Taylor. 1997. Cooperative activation of IP_3 receptors by sequential binding of IP_3 and Ca^{2+} safeguards against spontaneous activity. *Curr. Biol.* 7:510–518.

82. Foskett, J. K., C. White, …, D.-O. D. Mak. 2007. Inositol trisphosphate receptor Ca^{2+} release channels. *Physiol. Rev.* 87:593–658.

83. Siekmann, I., L. E. Wagner, 2nd, …, J. Sneyd. 2012. A kinetic model for type I and {II} {IP3R} accounting for mode changes. *Biophys. J.* 103:658–668.

84. Dupont, G., M. Falcke, …, J. Sneyd. 2016. Models of Calcium Signalling. *In* Interdisciplinary Applied Mathematics, *volume 43* Springer.

85. Bentele, K., and M. Falcke. 2007. Quasi-steady approximation for ion channel currents. *Biophys. J.* 93:2597–2608.

86. Falcke, M., and V. N. Friedhoff. 2018. The stretch to stray on time: Resonant length of random walks in a transient. *Chaos.* 28, 053117.

87. Dargan, S. L., and I. Parker. 2003. Buffer kinetics shape the spatiotemporal patterns of IP_3 -evoked Ca^{2+} signals. *J. Physiol. (London).* 553:775–788.

88. Dargan, S. L., B. Schwaller, and I. Parker. 2004. Spatiotemporal patterning of IP_3 -mediated Ca^{2+} signals in Xenopus oocytes by Ca^{2+} -binding proteins. *J. Physiol. (London).* 556:447–461.

89. Zeller, S., S. Rüdiger, …, M. Falcke. 2009. Modeling of the modulation by buffers of Ca^{2+} release through clusters of IP_3 receptors. *Biophys. J.* 97:992–1002.

90. Rooney, T. A., E. J. Sass, and A. P. Thomas. 1990. Agonsit-induced cytosolic calcium oscillations originate from a specific locus in single hepatocytes. *J. Biol. Chem.* 265:10792–10796.

91. Callamaras, N., J. S. Marchant, …, I. Parker. 1998. Activation and coordination of InsP 3-mediated elementary Ca^{2+} events during global Ca^{2+} signals in Xenopus oocytes. *J. Physiol.* 509:81–91.

92. Dickinson, G. D., and I. Parker. 2013. Factors determining the recruitment of inositol trisphosphate receptor channels during calcium puffs. *Biophys. J.* 105:2474–2484.

93. Lock, J. T., K. J. Alzayady, …, I. Parker. 2018. All three IP_3 receptor isoforms generate Ca^{2+} puffs that display similar characteristics. *Sci. Signal.* 11, eaau0344.

94. Mataragka, S., and C. W. Taylor. 2018. All three IP_3 receptor subtypes generate Ca^{2+} puffs, the universal building blocks of IP 3-evoked Ca^{2+} signals. *J. Cell Sci.* 131, Jcs220848.

95. Dupont, G., and A. Goldbeter. 1989. Theoretical Insights into the Origin of Signal Induced Ca^{2+} oscillations. Academic Press, London, pp. 449–459.

96. Tang, Y., J. L. Stephenson, and H. G. Othmer. 1996. Simplification and analysis of models of calcium dynamics based on IP_3-sensitive calcium channel kinetics. *Biophys. J.* 70:246–263.

97. Sneyd, J., M. Falcke, …, C. Fox. 2004. A comparison of three models of the inositol trisphosphate receptor. *Prog. Biophys. Mol. Biol.* 85:121–140.

98. Voorsluijs, V., S. P. Dawson, …, G. Dupont. 2019. Deterministic limit of intracellular calcium spikes. *Phys. Rev. Lett.* 122, 088101.

99. Sneyd, J., J. M. Han, …, D. I. Yule. 2017. On the dynamical structure of calcium oscillations. *Proc. Nat. Acad. Sci. USA.* 114:1456–1461.

100. Houart, G., G. Dupont, and A. Goldbeter. 1999. Bursting, chaos and birthmicity originating from self-modulation of the inositol 1,4,5-trisphosphate signal in a model for intracellular Ca^{2+} oscillations. *Bull. Math. Biol.* 61:507–530.

101. Höfer, T. 1999. Model of intercellular calcium oscillations in hepatocytes: synchronization of heterogeneous cells. *Biophys. J.* 77:1244–1256.

102. Kummer, U., L. F. Olsen, …, G. Baier. 2000. Switching from simple to complex oscillations in calcium signaling. *Biophys. J.* 79:1188–1195.

103. Dupont, G., G. Houart, and A. Goldbeter. 2003. From Simple to Complex Ca^{2+} oscillations: Regulatory Mechanisms and Theoretical Models. Springer, pp. 129–151, chapter 8, Lecture Notes in Physics, Vol. 623.

104. Schuster, S., M. Marhl, and T. Höfer. 2002. Modelling of simple and complex calcium oscillations. *Eur. J. Biochem.* 269:1333–1355.

105. Falcke, M. 2004. Reading the patterns in living cells - the Physics of Ca^{2+}signaling. *Adv. Phys.* 53:255–440.